Report

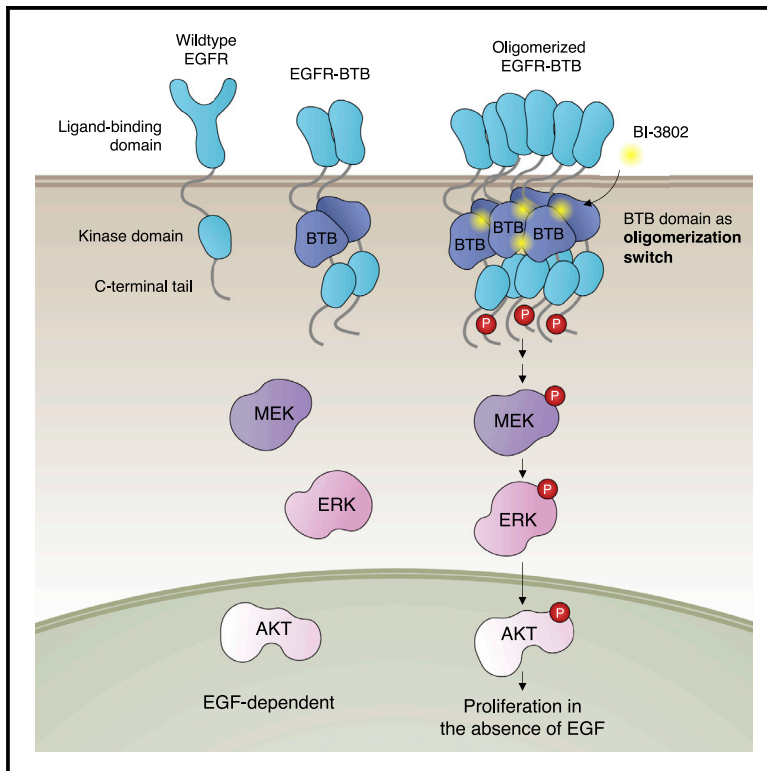# BTB$_{BCL6}$ dimers as building blocks for reversible drug-induced protein oligomerization

Graphical abstract

Authors

Lena Nitsch, Patrizia Jensen, Hojong Yoon, ..., Claudia Scholl, Stefan Fröhling, Mikołaj Słabicki

Correspondence

slabicki@broadinstitute.org

In brief

Protein oligomerization is a ubiquitous process in nature. Nitsch et al. characterize a minimal BTB$_{BCL6}$ domain that can be fused to a protein of choice to drive reversible oligomerization modulated by small molecules.

Highlights

- The BTB$_{BCL6}$ domain is a compound-triggered, reversible oligomerization switch

- Length of BTB$_{BCL6}$ oligomers is controlled by drug concentrations and treatment time

- Oligomerization of EGFR-BTB$_{BCL6}$ fusions induces downstream signaling in absence of EGF

CellPress

Report

BTB$_{BCL6}$ dimers as building blocks for reversible drug-induced protein oligomerization

Lena Nitsch,[1,9,10,11] Patrizia Jensen,[1,9] Hojong Yoon,[2,3,4,5] Jonas Koeppel,[1,6] Shourya Sonkar Roy Burman,[4,5] Eric Sebastian Fischer,[4,5] Claudia Scholl,[7] Stefan Fröhling,[1,8] and Mikołaj Słabicki[1,2,3,12,*]

[1]Division of Translational Medical Oncology, German Cancer Research Center (DKFZ) and National Center for Tumor Diseases (NCT), 69120 Heidelberg, Germany
[2]Broad Institute of MIT and Harvard, Cambridge, MA 02142, USA
[3]Department of Medical Oncology, Dana-Farber Cancer Institute, Boston, MA 02215, USA
[4]Department of Cancer Biology, Dana-Farber Cancer Institute, Boston, MA 02215, USA
[5]Department of Biological Chemistry and Molecular Pharmacology, Harvard Medical School, Boston, MA 02115, USA
[6]Wellcome Sanger Institute, Wellcome Genome Campus, Hinxton, UK
[7]Division of Applied Functional Genomics, German Cancer Research Center (DKFZ) and National Center for Tumor Diseases (NCT), 69120 Heidelberg, Germany
[8]German Cancer Consortium (DKTK), 69120 Heidelberg, Germany
[9]These authors contributed equally
[10]Present address: Berlin Institute of Health at Charité - Universitätsmedizin Berlin, Berlin, Germany
[11]Present address: Max-Delbrück-Center for Molecular Medicine in the Helmholtz Association (MDC), Berlin Institute for Medical Systems Biology (BIMSB), Berlin, Germany
[12]Lead contact
*Correspondence: slabicki@broadinstitute.org
https://doi.org/10.1016/j.crmeth.2022.100193

MOTIVATION Molecular switches are employed as synthetic biology tools to transition between at least two states. Here, we aimed to develop a reversible, drug-induced oligomerization switch. We characterized a minimal BTB$_{BCL6}$ fusion construct acting as a switch that can undergo multiple rounds of oligomerization/de-oligomerization by small molecules. When fused to EGFR, this system enables reversible activation of downstream signaling, resulting in enhanced cell proliferation.

SUMMARY

Here, we characterize the BTB domain of the transcription factor BCL6 (BTB$_{BCL6}$) as a small-molecule-controlled, reversible oligomerization switch, which oligomerizes upon BI-3802 treatment and de-oligomerizes upon addition of BI-3812. We show that the magnitude of oligomerization can be controlled *in vitro* by BI-3802 concentration and exposure time. In cellular models, exposure to BI-3802/BI-3812 can drive multiple cycles of foci formation consisting of BTB$_{BCL6}$ fused to EGFP, which are not degraded due to the lack of a degron. We generated an epidermal growth factor receptor (EGFR)-BTB$_{BCL6}$ fusion. Treatment with BI-3802, as an ON switch, induced EGFR-BTB$_{BCL6}$ phosphorylation and activation of downstream effectors, which could in part be reversed by the addition of BI-3812, as an OFF switch. Finally, BI-3802-induced oligomerization of the EGFR-BTB$_{BCL6}$ fusion enhanced proliferation of an EGF-dependent cell line in absence of EGF. These results demonstrate the successful application of small-molecule-induced, reversible oligomerization as a switch for synthetic biology.
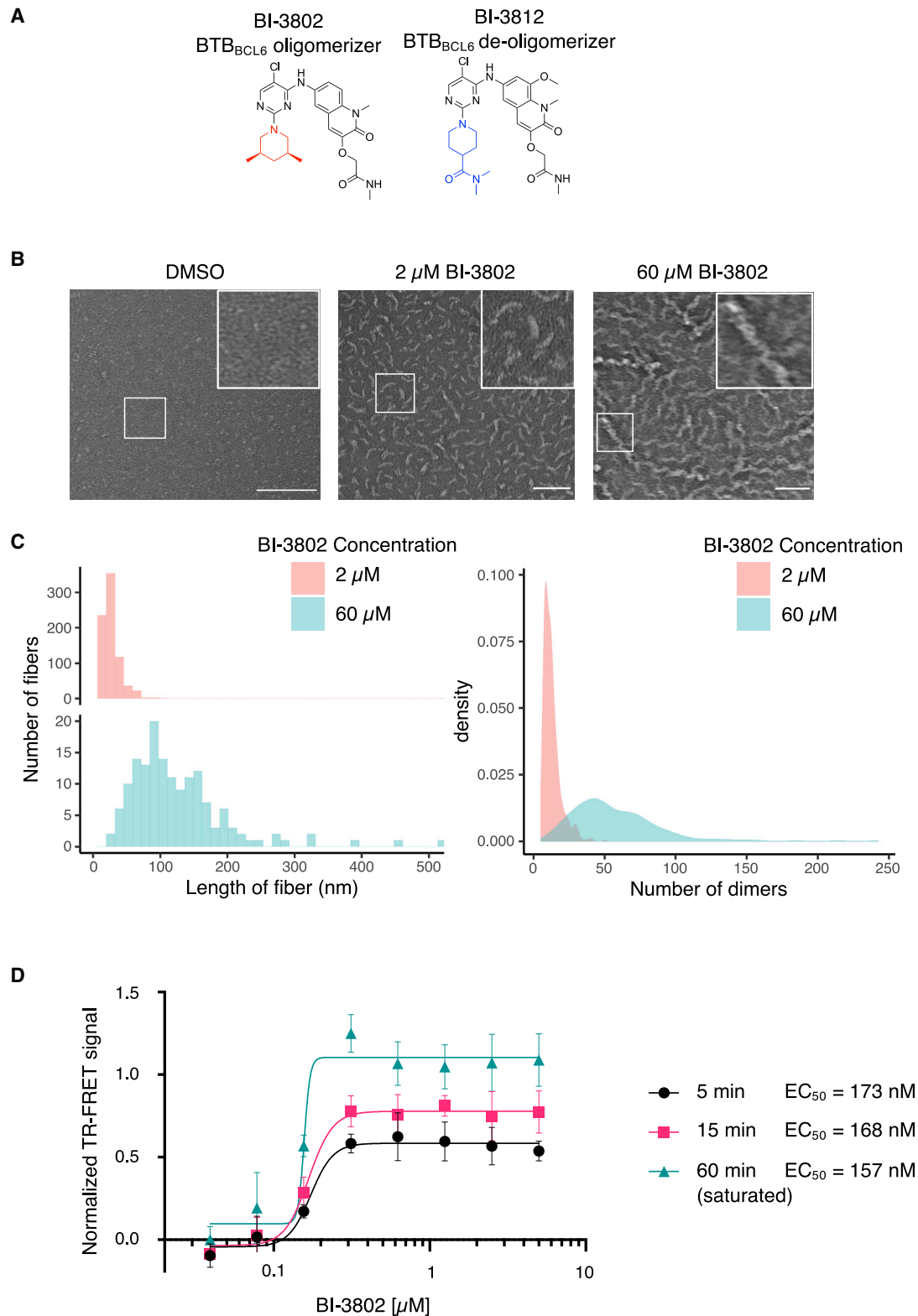
INTRODUCTION

Molecular switches can transition fast and reversibly between at least two states, enabling cellular adaptation in response to specific stimuli, such as changes in pH, light exposure, and ligand availability. Upon stimulation of membrane receptors, which can be classified as molecular switches, downstream signaling pathways are activated, resulting in altered gene expression. The withdrawal of stimuli may reverse this process; however, acute receptor inhibition could improve the temporal resolution of downstream signaling (Weber and Fussenegger, 2011).

Synthetic small molecules can replace physiological signals and specifically activate or inhibit cellular pathways. Such synthetic ligands can help understand downstream signaling and have applications in clinical areas such as chimeric

A

BI-3802
BTB$_{BCL6}$ oligomerizer

BI-3812
BTB$_{BCL6}$ de-oligomerizer

B

C

D

5 min   EC$_{50}$ = 173 nM

15 min   EC$_{50}$ = 168 nM

60 min   EC$_{50}$ = 157 nM
(saturated)

Figure 1. *In vitro* oligomerization by BI-3802 is dependent on compound concentration and treatment duration

(A) Chemical structures of the BCL6-oligomerizing compound BI-3802 and the BCL6-de-oligomerizing compound BI-3812, which were previously published as BCL6 degrader and inhibitor, respectively by Kerres et al. (2017). Solvent-exposed moieties, which determine the compounds' mechanisms of action, are highlighted in red and blue, respectively.

(legend continued on next page)

antigen receptor (CAR) T cell therapy (Labanieh et al., 2018). However, since only a limited number of synthetic switching systems show reversibility, there is a need to expand the repertoire of chemically engineered switches, which would enable multiple rounds of ON and OFF states (Weber and Fussenegger, 2011).

Oligomerization changes cellular responses to extra- or intracellular signals. Membrane-bound receptors can be differentially activated, leading to the initiation of various signal transduction processes (Gwyther et al., 2019). For example, the epidermal growth factor receptor (EGFR) initially dimerizes and subsequently oligomerizes upon stimulation, and only oligomeric receptors efficiently induce phosphorylation and activation of downstream signaling (Liang et al., 2018), particularly the mitogen-activated protein kinase (MAPK) and PI3K-AKT pathways (Wee and Wang, 2017). MAPK signaling involves phosphorylation and activation of a cascade of kinases, including MEK1/2, which in turn phosphorylate ERK1/2, which translocate to the nucleus to regulate transcription (Guo et al., 2020). A major player in the PI3K-AKT cascade is the AKT serine-threonine kinase, which, upon activation, modulates the function of several downstream targets, including proteins essential for proliferation, protein synthesis, and metabolism (King et al., 2015). Activation of both pathways shapes critical cellular responses to extracellular stimuli, resulting in proliferation, differentiation, and cell growth (Guo et al., 2020; King et al., 2015).

Protein oligomerization can also induce protein degradation by increasing the local concentration of E3 ubiquitin ligases and their substrates. Drug screens targeting the oncogenic transcription factor BCL6 revealed two compounds, BI-3802 and BI-3812, that bind to the groove formed by BTB_{BCL6} dimerization (Kerres et al., 2017). We subsequently showed that BI-3802 induces BCL6 oligomerization *in vivo* and *in vitro*, leading to its rapid ubiquitination and degradation (Kerres et al., 2017; Slabicki et al., 2020). In contrast, the structurally related non-degrading BCL6 inhibitor BI-3812 cannot form BTB_{BCL6} oligomers due to the presence of a dimethyl amide moiety, which would sterically clash in oligomers induced by BI-3802 (Figure 1A). Increased concentrations of BI-3812 can outcompete BI-3802 and, due to a steric clash of the solvent-exposed moiety, reverse BCL6 oligomerization. BTB_{BCL6} is sufficient for BI-3802-induced oligomerization but is not degraded due to the lack of degrons for the E3 ligases (Slabicki et al., 2020).

We here characterized minimal BTB_{BCL6} fusion constructs as non-degradable modular switches that can undergo multiple rounds of reversible oligomerization upon BI-3802/BI-3812 treatment. This system provides a tool to trigger reversible signaling events with precise temporal control.

RESULTS

Formation of BTB_{BCL6} foci is concentration and time dependent *in vitro*
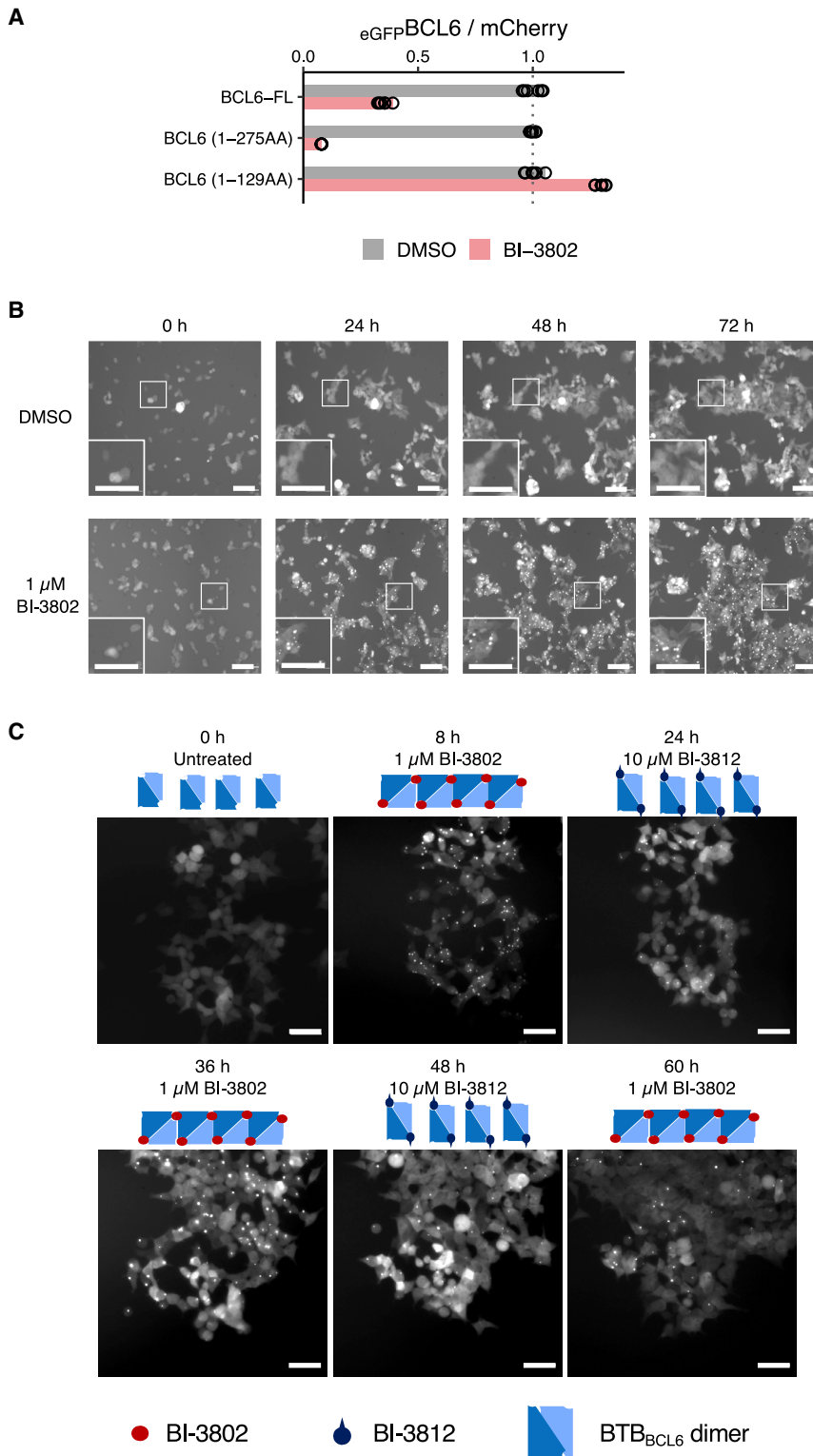
Before fusing BTB_{BCL6} to other functional domains, we sought to determine whether it is possible to control the degree of BTB_{BCL6} oligomerization. To this end, we performed negative stain electron microscopy with various BI-3802 concentrations. Without BI-3802, BTB_{BCL6} formed monodisperse dimer particles, but with an excess of BI-3802 (60 μM), BTB_{BCL6} formed long filaments (median length of ~110 nm, corresponding to 52 dimer particles) (Figures 1B and 1C). Decreasing the concentration of BI-3802 to 2 μM generated shorter filaments (median length of ~24 nm, corresponding to 11 dimer particles) (Figures 1B and 1C).

To characterize the kinetics of BI-3802-induced BTB_{BCL6} oligomerization, we developed an *in vitro* time-resolved fluorescence energy transfer (TR-FRET) assay. *In vitro* oligomerization is a rapid process, and we detected a concentration-dependent signal within 5 min of BI-3802 exposure, which increased to saturation after 60 min, corresponding to a half maximal effective concentration (EC_{50}) of 157 nM (Figure 1D). Together, *in vitro* characterization indicated that the length of BI-3802-induced BTB_{BCL6} filaments can be controlled by both drug dose and treatment duration.

EGFP-BTB_{BCL6} efficiently forms non-degraded intracellular foci as a surrogate of oligomerization

Previously, we observed the formation of EGFP-containing foci in cellular assays after adding BI-3802 to a reporter cell line expressing amino acids 1–275 or 1–250 of BCL6 fused to EGFP. The longer, 275-amino-acid construct is rapidly degraded upon oligomerization because it contains a VxP amino acid motif, which is a degron for the E3 ligase SIAH1. While the shorter, 250-amino-acid construct does not contain the VxP degron, we still noticed a slight decrease in protein levels after prolonged BI-3802 treatment (Slabicki et al., 2020). To generate a more compact, non-degradable BI-3802-inducible oligomerization switch, we fused the first 129 amino acids of BCL6, corresponding to its BTB domain, to EGFP and expressed this construct in HEK293T cells. The EGFP signal is a surrogate for BTB_{BCL6} protein levels and, simultaneously, allowed tracking of its subcellular localization. This minimal EGFP-BTB_{BCL6} construct was not degraded even after 3 days of BI-3802 treatment due to the lack of a degron (Figure 2A). To verify that it was still capable of oligomerization, we exposed the HEK293T reporter cell line to BI-3802 and tracked EGFP expression by fluorescence microscopy over 3 days. BI-3802 efficiently induced EGFP-BTB_{BCL6} foci throughout the experiment with no evidence of degradation (Figure 2B and S2). Together, these experiments demonstrate the formation of stable cellular BTB_{BCL6} foci, persisting over several days of BI-3802 treatment.

(B) Negative stain electron microscopy images of BCL6 (amino acids 5–360) in the presence of DMSO, 2 μM BI-3802, or 60 μM BI-3802. Scale bars, 100 nm; n > 10 images. For higher magnifications, zoom-in images are shown on the upper right corner of each image.

(C) Quantification of the distribution of fiber lengths observed by negative stain electron microscopy (Figure 1B) in the presence of 2 μM or 60 μM BI-3802 (left). Kernel density estimation of dimer numbers observed by negative stain electron microscopy after addition of 2 μM or 60 μM BI-3802 (right).

(D) Pre-assembled Bodipy-labeled and biotinylated BCL6 (amino acids 5–360) were treated with increasing concentrations of BI-3802, and the signal was measured by TR-FRET. Dots represent the mean. Lines represent the standard four-parameter log-logistic curve fit (n = 3). Error bars indicate SD.

A

B

C

● BI-3802   ◖ BI-3812   ◣◤ BTB_{BCL6} dimer

Cycles of BI-3802/BI-3812 induce BTB_{BCL6} oligomerization/de-oligomerization

BI-3812 is a close analog of BI-3802 (Figure 1A) that occupies the same binding pocket in BCL6 but does not

Figure 2. Alternating treatment with BI-3802 and BI-3812 enables cyclic oligomerization and de-oligomerization of an EGFP-BTB_{BCL6} fusion protein

(A) Flow cytometric analysis of HEK293T cells expressing full-length BCL6 (BCL6-FL) and two truncated BCL6 proteins containing amino acids 1–275 [BCL6 (1–275 AA)] and 1–129 [BCL6 (1–129 AA)], each coupled to EGFP, and treated with DMSO or 1 μM BI-3802 for 3 days. Fluorescence values are normalized to the DMSO control. Bars represent the mean of three independent experiments.

(B) Fluorescence live-cell microscopy of EGFP-BCL6 (1–129 AA) localization in HEK293T cells treated with DMSO or 1 μM BI-3802 for 3 days. White dots are due to foci formation of EGFP-BCL6 (1–129 AA). Images acquired at 0, 48, 72, and 96 h are shown. Additional time points are provided in Figure S1. Scale bar, 100 μm. Magnification, 10×; for higher magnification, zoom-in images are shown on the lower-left corner of each image.

(C) Fluorescence live-cell microscopy of EGFP-BCL6 (1–129 AA) localization in HEK293T cells treated with successive cycles of 1 μM BI-3802 and 10 μM BI-3812 without cell washing. White dots are due to foci formation of EGFP-BCL6 (1–129 AA). After every image acquisition, cell culture medium was replaced with fresh medium containing the indicated compound. Scale bar, 50 μm. Magnification, 10×. Schematics illustrate reversible BCL6_{BTB} oligomerization: In the absence of drug, two BCL6_{BTB} dimerize; addition of BI-3802 (red) causes BCL6_{BTB} oligomerization; excess of BI-3812 leads to de-oligomerization of BCL6_{BTB} foci.

oligomerize BCL6, thus enabling BCL6 de-oligomerization (Kerres et al., 2017). To test if EGFP-BTB_{BCL6} can be employed as an ON/OFF molecular switch, we exposed the reporter cell line to two rounds of BI-3802 and subsequent BI-3812 treatment and monitored EGFP-BTB_{BCL6} localization by fluorescence live-cell microscopy. EGFP-BTB_{BCL6} showed a diffuse cellular localization in untreated cells. BI-3802 efficiently induced the formation of cytoplasmic BTB_{BCL6} foci after 8 h, which was reversed by the replacement of BI-3802 with excess BI-3812 for 16 h. Small molecule-induced oligomerization and de-oligomerization were achieved in two additional cycles but with decreased efficiency in the last round of BI-3812 treatment (Figure 2C). To further characterize the kinetics of a single round of de-oligomerization, cells with BI-3802-induced foci were treated with BI-3812. After 10 min and 2 h of BI-3812 exposure, 47% and 6% of foci were still detectable, respectively, indicating rapid de-oligomerization in
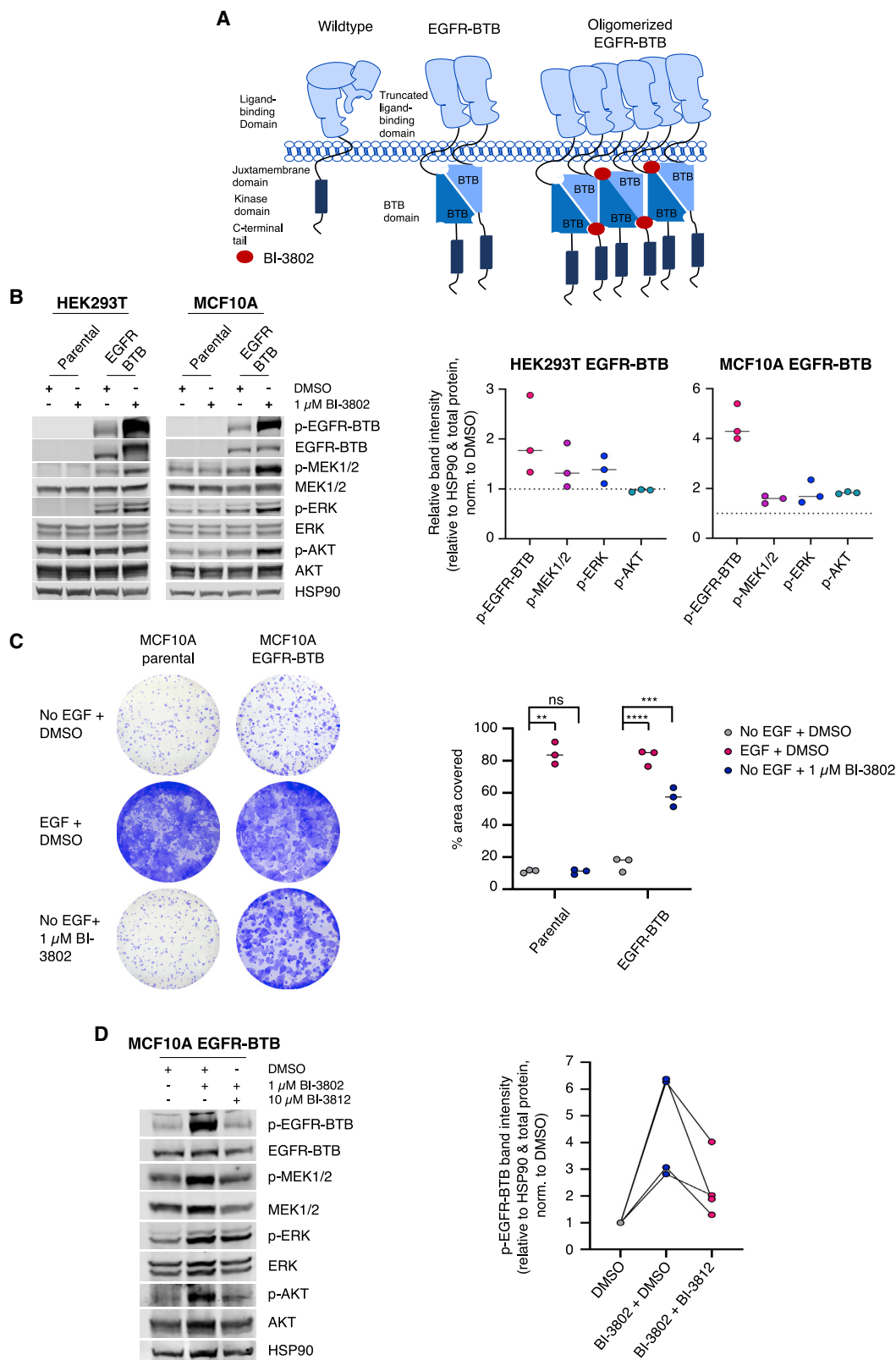
(legend on next page)

the cellular system (Figure S2C). In aggregate, these results demonstrate that BTB$_{BCL6}$ can be employed as a reversible oligomerization switch that is not degraded upon prolonged BI-3802 treatment through cycles of oligomerization and de-oligomerization.

EGFP-EGFR-BTB$_{BCL6}$ fusions induce downstream signaling and EGF-independent proliferation upon BI-3802 treatment

To investigate whether BTB$_{BCL6}$ can induce oligomerization and activation of receptors, we designed an EGFP-EGFR expression construct in which the BTB$_{BCL6}$ domain was inserted between the receptor's transmembrane and kinase domains with a truncated ligand-binding domain (Figure 3A). We chose EGFR as a model because its downstream effectors are well characterized and because of its oncogenic potential in various tissues. We introduced the EGFP-EGFR-BTB$_{BCL6}$ construct via lentiviral transduction into HEK293T cells and MCF10A mammary epithelial p53$^{-/-}$ cells (referred to as MCF10A hereafter), whose proliferation is highly dependent on the EGF-EGFR signaling axis (Tang et al., 2014), and confirmed stable expression and membrane localization of the EGFP-BTB$_{BCL6}$-coupled receptor in both cell lines (Figure S3A).

To evaluate the activity of the fusion receptor after oligomerization by BI-3802, we analyzed the phosphorylation of EGFR and components of two downstream signaling pathways, i.e., the RAS-MAPK and PI3K-AKT cascades. We first assessed the phosphorylation of the fusion receptor at different time points and in the presence of varying BI-3802 concentrations and found that the signal was optimal after treatment with 1 μM BI-3802 (Figure S3B). After 10 min of BI-3802 treatment, both reporter cell lines showed increased phosphorylation of the EGFR-BTB$_{BCL6}$ fusion protein and of MEK1/2 and ERK1/2 (Figure 3B), demonstrating rapid activation of the RAS-MAPK signaling axis. In addition, BI-3802 induced strong AKT phosphorylation in MCF10A cells, indicating activation of the PI3K-AKT pathway. BI-3802 treatment of the parental cell lines lacking an EGFR-BTB$_{BCL6}$ fusion did not induce phosphorylation of any of these signaling proteins (Figure 3B), confirming the specificity of BI-3802 for BTB$_{BCL6}$. Together, these experiments demonstrate the successful activation of EGFR effector pathways by small-molecule-induced oligomerization of an EGFR-BTB$_{BCL6}$ fusion protein.

MCF10A cells depend on the EGF-EGFR signaling axis for proliferation (Tang et al., 2014). To assess if EGFR-BTB$_{BCL6}$ oligomerization and subsequent pathway activation are sufficient to sustain proliferation of MCF10A cells in the absence

of EGF, we performed colony-formation assays with parental and EGFR-BTB$_{BCL6}$-expressing MCF10A cells in the presence of BI-3802 or EGF as control. BI-3802 significantly enhanced the proliferation of EGFR-BTB$_{BCL6}$-expressing cells cultured without EGF to a level closely resembling the effect of EGF (Figure 3C). In contrast, parental MCF10A cells did not show increased proliferation after BI-3802 treatment, confirming that the molecule acts specifically on BTB$_{BCL6}$ (Figure 3C). These data indicate that the EGFR-BTB$_{BCL6}$ fusion protein is functional and capable of inducing downstream signaling upon activation by BI-3802, resulting in increased cell proliferation that phenocopies the effect of the physiological ligand EGF. Our results also suggest that this synthetic switch can serve as a tool for manipulating and rewiring central signaling pathways.

EGFR-BTB$_{BCL6}$ phosphorylation can be switched off by BI-3812

Since BI-3812 can revert BI-3802-induced BTB$_{BCL6}$ oligomerization (Figure 3D), we sought to evaluate if it can also dissolve oligomerized EGFR-BTB$_{BCL6}$ fusion proteins, thereby abrogating EGFR downstream signaling as an OFF switch. We treated MCF10A cells expressing EGFR-BTB$_{BCL6}$ with BI-3802 for 3 min and subsequently added BI-3812. Immunoblotting showed that phosphorylation of the EGFR-BTB$_{BCL6}$ fusion was reversed in less than 10 min after BI-3812 addition, which was accompanied by a moderate reduction in phosphorylation of the EGFR downstream effectors MEK, ERK, and AKT (Figure 3D). These findings demonstrate that the EGFR-BTB$_{BCL6}$ fusion functions as a switch whose activity can be precisely regulated by adding and withdrawing BI-3802 and BI-3812.

DISCUSSION

Building on our previous work (Slabicki et al., 2020), we characterized a minimal BTB$_{BCL6}$ domain of which oligomerization can be controlled by the concentration and exposure time of BI-3802. The addition of the close analog BI-3812 solubilized BI-3802-induced foci and enabled multiple rounds of drug-induced foci formation and resolution. The reversibility of the BTB$_{BCL6}$ switch is currently limited to a few cycles of foci formation, and it might require further engineering of the BTB domain's protein sequence and the small molecule to improve this property. Nevertheless, our results demonstrate that BTB$_{BCL6}$, paired with BI-3802 and BI-3812, can be employed as a reversible molecular switch and presents a unique opportunity to temporally control biological processes

---

Figure 3. BI-3802 oligomerizes and activates an EGFR-BTB$_{BCL6}$ fusion protein and enhances EGFR downstream signaling and cell proliferation

(A) Schematic of wild-type EGFR and the EGFR-BTB$_{BCL6}$ fusion receptor.

(B) Parental and EGFR-BTB$_{BCL6}$-expressing HEK293T and MCF10A cells were treated with 1 μM BI-3802 or DMSO for 10 min. Protein expression and phosphorylation were assessed by immunoblotting. (left panel). Band intensities of phosphorylated proteins were quantified and normalized to the respective total protein and loading control (HSP90) (right panel). Dashed lines indicate the DMSO control. n = 3, see Figure S3D for replicate blots.

(C) Parental and EGFR-BTB$_{BCL6}$-expressing MCF10A cells were cultured with the indicated combinations of DMSO, EGF, and 1 μM BI-3802 for 7 days. Colonies were visualized with 2.5% crystal violet (left panel) and quantified (right panel). **p < 0.01, ***p < 0.001, ****p < 0.0001. ns, not significant. n = 3.

(D) MCF10A cells expressing EGFR-BTB$_{BCL6}$ were treated with DMSO for 10 min, 1 μM BI-3802 for 10 min, or 1 μM BI-3802 for 3 min and 10 μM BI-3812 for an additional 7 min (left panel). Phosphorylation of the receptor and downstream signaling proteins was assessed using immunoblotting (left panel). For quantification, proteins were normalized to HSP90, and the ratio of phosphorylated to total protein was determined for EGFR (right panel). n = 4, see Figure S3E for additional replicates.

triggered by oligomerization of signaling nodes. Various types of synthetic switches have been reported previously (Brenner et al., 2018); however, BTB$_{BCL6}$ is a unique switch in that it allows us to increase the local concentration of proteins, which will be crucial for dissecting the biological consequences of oligomerization for any domains or proteins of interest.

As a proof of concept, we applied this system in the biological context of receptor tyrosine kinase signaling. We stably expressed an EGFR-BTB$_{BCL6}$ fusion protein in two human cell lines and observed that the oligomerized EGFR by the treatment with BI-3802 resulted in the activation of the fusion receptor itself and its downstream pathways, including RAS-MAPK and PI3K-AKT signaling. This intracellular response translated into changes in cellular behavior, such as an EGF-independent proliferation of MCF10A cells, which requires EGFR signaling for their growth and proliferation (Tang et al., 2014). Conversely, the de-oligomerization of EGFR-BTB$_{BCL6}$ by BI-3812 treatment resulted in rapid dephosphorylation of EGFR-BTB$_{BCL6}$, and a moderate decrease in the phosphorylation of downstream kinases. Together, these observations demonstrate that signaling pathways affected by the oligomerization of their components can be modulated by fusing BTB$_{BCL6}$ as an oligomerization tag, and we envision that the EGFR-BTB$_{BCL6}$ system can be used in combination with other switches, resulting in more complex synthetic circuits.

We previously showed that BI-3802-induced oligomerization leads to the degradation of BCL6 due to the recruitment of an E3 ligase that recognizes a degron motif outside the BTB domain (Slabicki et al., 2020). Fusion of the BTB$_{BCL6}$ switch to another protein with an accessible degron could trigger unintended construct degradation and thereby loss of the protein of interest. Thus, careful examination is needed before applying this fusion tag-based oligomerization system for dissecting the downstream effects of target protein oligomerization. To avoid potential structural clashes, BTB$_{BCL6}$ should be fused to other protein domains via flexible linkers (GGGGSGGGGS in our design). Fusion construct geometry and linker length might have an impact on downstream effects and activity. It is also possible that the BTB$_{BCL6}$ fusion may form hetero-oligomers with endogenous BCL6 upon BI-3802 treatment, which might lead to degradation of the fusion construct. Employing the BTB$_{BCL6}$ fusion as an oligomerization switch would thus be ideal for cell lines that do not express or are not dependent on BCL6 (Kerres et al., 2017). Treatment of BCL6-dependent cell lines with BI-3802 or BI-3812 would further reduce their proliferation due to loss of endogenous BCL6. However, more than 99% of cell lines characterized in the Cancer Dependency Map project do not require BCL6 (Meyers et al., 2017).

Drug-induced protein-protein interaction can be mediated by various compounds, including rapamycin, which brings FRB and FKBP binding sites into proximity (Banaszynski et al., 2005). By creative assembly of these sites, rapamycin might also be employed for protein oligomerization (Inobe and Nukina, 2016). These previous drugs introduced monomer-monomer interactions. Since the BTB$_{BCL6}$ domain is an obligate homodimer, our system induces switchable dimer-dimer oligomerization, which makes it ideal for investigating the effectors of other known homo-oligomeric proteins, such as many receptor tyrosine kinases. More-

over, no switchable methods are available to control the formation and dissociation of oligomeric proteins, which recapitulate oligomeric status-based nascent regulatory mechanisms in cells.

Thalidomide analogs such as lenalidomide induce proximity between the CRL4^{CRBN} E3 ubiquitin ligase and the zinc finger degron-containing transcription factors IKZF1/3 (Kronke et al., 2015). Engineering of these molecular components allowed the construction of an ON and OFF switch-based system for controlling the effector functions of CAR T cells using lenalidomide (Jan et al., 2021). These switches induce dimerization instead of oligomerization. However, the formation of an immunological synapse requires clustering of many T cell receptors (Lee et al., 2003), and it would be interesting to compare the effects of the thalidomide analog-induced CRBN-IKFZ1/3 dimerization switch with those of a BI-3802-induced BTB$_{BCL6}$ oligomerization switch.

In summary, we have developed a novel chemical and synthetic biology tool to investigate the functional consequences of protein oligomerization in a precisely regulatable manner. Given its fast reversibility and high substrate specificity (Kerres et al., 2017; Slabicki et al., 2020), this system can be used to broaden our understanding of cellular signaling networks, e.g., by studying the function of orphan receptors with unknown ligands, such as ERBB2 (Serova et al., 2019). Beyond oligomerization of signaling modules, we envision that the BTB$_{BCL6}$ switch also could be employed more generally to investigate the effects of increased local protein concentrations, such as those proposed for biomolecular condensates (Feng et al., 2019).

LIMITATIONS OF THE STUDY

A protein domain of interest needs to be fused to the BTB$_{BCL6}$ switch with flexible linkers to avoid a potential structural clash that could prevent oligomerization or impair the function of the fusion partner. Since BI-3802 was described to degrade full-length BCL6 (Slabicki et al., 2020), fusion constructs containing a degron motif outside the BTB$_{BCL6}$ domain could potentially be degraded. Finally, to avoid undesired effects due to BI-3802-induced degradation of endogenous BCL6 or BTB$_{BCL6}$ switch dimerization with endogenous BCL6, it is advised to express BTB$_{BCL6}$ fusion constructs in cell lines that neither express nor depend on BCL6.

STAR★METHODS

Detailed methods are provided in the online version of this paper and include the following:

- KEY RESOURCE TABLE
- RESOURCE AVAILABILITY
  - ○ Lead contact
  - ○ Material availiability
  - ○ Data and code availability
- EXPERIMENTAL MODEL AND SUBJECT DETAILS
  - ○ Cell lines
  - ○ Microbe stains
- METHOD DETAILS
  - ○ Construct design
  - ○ Negative stain

REFERENCES

Banaszynski, L.A., Liu, C.W., and Wandless, T.J. (2005). Characterization of the FKBP.rapamycin.FRB ternary complex. J. Am. Chem. Soc. *127*, 4715–4721. https://doi.org/10.1021/ja043277y.

Brenner, M.J., Cho, J.H., Wong, N.M.L., and Wong, W.W. (2018). Synthetic biology: immunotherapy by design. Annu. Rev. Biomed. Eng. *20*, 95–118. https://doi.org/10.1146/annurev-bioeng-062117-121147.

Feng, Z., Chen, X., Wu, X., and Zhang, M. (2019). Formation of biological condensates via phase separation: characteristics, analytical methods, and physiological implications. J. Biol. Chem. *294*, 14823–14835. https://doi.org/10.1074/jbc.REV119.007895.

Guo, Y.J., Pan, W.W., Liu, S.B., Shen, Z.F., Xu, Y., and Hu, L.L. (2020). ERK/MAPK signalling pathway and tumorigenesis. Exp. Ther. Med. *19*, 1997–2007. https://doi.org/10.3892/etm.2020.8454.

Gwyther, R.E.A., Jones, D.D., and Worthy, H.L. (2019). Better together: building protein oligomers naturally and by design. Biochem. Soc. Trans. *47*, 1773–1780. https://doi.org/10.1042/BST20190283.

Inobe, T., and Nukina, N. (2016). Rapamycin-induced oligomer formation system of FRB-FKBP fusion proteins. J. Biosci. Bioeng. *122*, 40–46. https://doi.org/10.1016/j.jbiosc.2015.12.004.

Jan, M., Scarfo, I., Larson, R.C., Walker, A., Schmidts, A., Guirguis, A.A., Gasser, J.A., Slabicki, M., Bouffard, A.A., Castano, A.P., et al. (2021). Reversible ON- and OFF-switch chimeric antigen receptors controlled by lenalidomide. Sci. Transl. Med. *13*, eabb6295. https://doi.org/10.1126/scitranslmed.abb6295.

Kerres, N., Steurer, S., Schlager, S., Bader, G., Berger, H., Caligiuri, M., Dank, C., Engen, J.R., Ettmayer, P., Fischerauer, B., et al. (2017). Chemically induced degradation of the oncogenic transcription factor BCL6. Cell Rep. *20*, 2860–2875. https://doi.org/10.1016/j.celrep.2017.08.081.

King, D., Yeomanson, D., and Bryant, H.E. (2015). PI3King the lock: targeting the PI3K/Akt/mTOR pathway as a novel therapeutic strategy in neuroblastoma. J. Pediatr. Hematol. Oncol. *37*, 245–251. https://doi.org/10.1097/Mph.0000000000000329.

Kronke, J., Fink, E.C., Hollenbach, P.W., MacBeth, K.J., Hurst, S.N., Udeshi, N.D., Chamberlain, P.P., Mani, D.R., Man, H.W., Gandhi, A.K., et al. (2015). Lenalidomide induces ubiquitination and degradation of CK1alpha in del(5q) MDS. Nature *523*, 183–188. https://doi.org/10.1038/nature14610.

Labanieh, L., Majzner, R.G., and Mackall, C.L. (2018). Programming CAR-T cells to kill cancer. Nat. Biomed. Eng. *2*, 377–391. https://doi.org/10.1038/s41551-018-0235-9.

Lee, K.H., Dinner, A.R., Tu, C., Campi, G., Raychaudhuri, S., Varma, R., Sims, T.N., Burack, W.R., Wu, H., Wang, J., et al. (2003). The immunological synapse balances T cell receptor signaling and degradation. Science *302*, 1218–1222. https://doi.org/10.1126/science.1086507.

Liang, S.I., van Lengerich, B., Eichel, K., Cha, M., Patterson, D.M., Yoon, T.Y., von Zastrow, M., Jura, N., and Gartner, Z.J. (2018). Phosphorylated EGFR dimers are not sufficient to activate Ras. Cell Rep. *22*, 2593–2600. https://doi.org/10.1016/j.celrep.2018.02.031.

Meyers, R.M., Bryan, J.G., McFarland, J.M., Weir, B.A., Sizemore, A.E., Xu, H., Dharia, N.V., Montgomery, P.G., Cowley, G.S., Pantel, S., et al. (2017). Computational correction of copy number effect improves specificity of CRISPR-Cas9 essentiality screens in cancer cells. Nat. Genet. *49*, 1779–1784. https://doi.org/10.1038/ng.3984.

The PyMOL Molecular Graphics System (2010). Version 2.5.1 Schrödinger (LLC).

Nowak, R.P., DeAngelo, S.L., Buckley, D., He, Z., Donovan, K.A., An, J., Safaee, N., Jedrychowski, M.P., Ponthier, C.M., Ishoey, M., et al. (2018). Plasticity in binding confers selectivity in ligand-induced protein degradation. Nat. Chem. Biol. *14*, 706–714. https://doi.org/10.1038/s41589-018-0055-y.

Scheres, S.H. (2012). RELION: implementation of a Bayesian approach to cryo-EM structure determination. J. Struct. Biol. *180*, 519–530. https://doi.org/10.1016/j.jsb.2012.09.006.

Serova, O.V., Chachina, N.A., Gantsova, E.A., Popova, N.V., Petrenko, A.G., and Deyev, I.E. (2019). Autophosphorylation of orphan receptor ERBB2 can Be induced by extracellular treatment with mildly alkaline media. Int. J. Mol. Sci. *20*, 1515. https://doi.org/10.3390/ijms20061515.

Cell Reports Methods
Report

Slabicki, M., Yoon, H., Koeppel, J., Nitsch, L., Roy Burman, S.S., Di Genua, C., Donovan, K.A., Sperling, A.S., Hunkeler, M., Tsai, J.M., et al. (2020). Small-molecule-induced polymerization triggers degradation of BCL6. Nature *588*, 164–168. https://doi.org/10.1038/s41586-020-2925-1.

Tang, W.Y.Y., Beckett, A.J., Prior, I.A., Coulson, J.M., Urbe, S., and Clague, M.J. (2014). Plasticity of mammary cell boundaries governed by EGF and actin Remodeling. Cell Rep. *8*, 1722–1730. https://doi.org/10.1016/j.celrep.2014.08.026.

Weber, W., and Fussenegger, M. (2011). Molecular diversity–the toolbox for synthetic gene switches and networks. Curr. Opin. Chem. Biol. *15*, 414–420. https://doi.org/10.1016/j.cbpa.2011.03.003.

Wee, P., and Wang, Z. (2017). Epidermal growth factor receptor cell proliferation signaling pathways. Cancers (Basel) *9*, 52. https://doi.org/10.3390/cancers9050052.

Zivanov, J., Nakane, T., and Scheres, S.H.W. (2020). Estimation of high-order aberrations and anisotropic magnification from cryo-EM data sets in RELION-3.1. IUCrJ *7*, 253–267. https://doi.org/10.1107/S2052252520000081.

STAR★METHODS

KEY RESOURCE TABLE

REAGENT or RESOURCE	SOURCE	IDENTIFIER
Antibodies		
Anti-phospho-Akt (S473)	Cell Signaling Technology	#9271
anti-Akt	Cell Signaling Technology	#2920
anti-p44/42 MAPK (Erk1/2)	Cell Signaling Technology	#9102
anti-phospho-Erk1/2 (T202/204)	Cell Signaling Technology	#4370
anti-EGFR	Cell Signaling Technology	#4267
anti-phospho-EGFR (Y1068)	Cell Signaling Technology	#3777
anti-GFP	Cell Signaling Technology	#2956
anti-MEK1/2	Cell Signaling Technology	#4694
anti-phospho-Mek1/2 (S217/221)	Cell Signaling Technology	#9154
anti-HSP90a/b	Santa Cruz Biotechnology	#sc-13119
DyLight-conjugated secondary antibodies	Cell Signaling Technology	#5470
DyLight-conjugated secondary antibodies	Cell Signaling Technology	#5151
DyLight-conjugated secondary antibodies	Cell Signaling Technology	#5366
DyLight-conjugated secondary antibodies	Cell Signaling Technology	#5257
Bacterial and virus strains		
Stbl3	Claudia Scholl	N/A
MAX Efficiency™ DH5α Competent Cells	Invitrogen	#18258012
pAAV-CAG-EGFR-BTB	This paper	N/A
Chemicals, peptides, and recombinant proteins		
BI-3802	opnMe	N/A
BI-3812	opnMe	N/A
Strep·Tag II-Avi–BCL6 (amino acids 5-360)	Slabicki et al., 2020	N/A
His$_6$-BCL6-Spytag (amino acids 5-360)	Slabicki et al., 2020	N/A
BodipyFL-labeled Spycatcher	Nowak et al., 2018	N/A
LanthaScreen™ Tb-Streptavidin, 1 mg/m	Invitrogen	PV3966
Bodipy-FL Maleimide	ThermoFisher Scientific	B10250
Experimental models: Cell lines		
HEK293T cells	ATCC	CRL-3216
MCF10A p53−/− cells	Claudia Scholl	N/A
HEK293T-EGFR-BTB	This paper	N/A
MCF10a-EGFR-BTB	This paper	N/A
Sf9 cells	ATCC	CRL-1711
High Five™ cells	ThermoFisher Scientific	B85502
Recombinant DNA		
pArtichoke	Addgene	#73320
pArtichoke-EGFR-BTB	This paper	N/A
pAC8-STREP II-Avi tag-BCL6 (5-360)	Slabicki et al., 2020	N/A
pAC8-His$_6$-BCL6-Spytag (5-360)	Slabicki et al., 2020	N/A
Software and algorithms		
GraphPad Prism (version 8.4.2)	GraphPad Software, Inc	https://www.graphpad.com/scientific-software/prism/
ImageJ	National Institutes of Health, USA	https://imagej.nih.gov/ij/
Leica Application Suite X Software	Leica	N/A

Continued

REAGENT or RESOURCE	SOURCE	IDENTIFIER
RELION 3.1	(Scheres, 2012; Zivanov, Nakane and Scheres, 2020)	https://relion.readthedocs.io/en/release-3.1/
PyMOL 2.5.1	Schrödinger	https://pymol.org/2/
R	The R Foundation	https://www.r-project.org/
Other		
FuGene HD transfection reagent	Promega	4561096
ESF921 insect cell culture medium	Expression Systems	10437-028
Sf-900 II SFM serum-free medium, complete	Gibco	E2311
Vivaspin Turbo 4, 30,000 MWCO concentrator	Sartorius	96-001-01
Strep-TactinXT Superflow high capacity	IBA	10902-088
Superdex 200 Increase 10/300 GL	GE Healthcare	VS04T21
PHERAstar FS microplate reader	BMG Labtech	N/A
Carbon-coated nickel grid	Electron Microscopy Science	CF400-Ni-UL
JEOL JEM 1400plus	Jeol	N/A

RESOURCE AVAILABILITY

Lead contact
Further information and requests for resources and reagents should be directed to and will be fulfilled by the lead contact, Mikołaj Słabicki (slabicki@broadinstitute.org).

Material availiability
Plasmids and all unique reagents generated in this study are available from the lead contact with a completed material transfer agreement.

Data and code availability
- All data reported in this paper will be shared by the lead contact upon request.
- This paper does not report original code.
- Any additional information required to reanalyze the data reported in this paper is available from the lead contact upon request.

EXPERIMENTAL MODEL AND SUBJECT DETAILS

Cell lines
HEK293T cells were obtained from the American Type Culture Collection. MCF10A p53−/− cells were a gift from Claudia Scholl. HEK293T cells were cultured in DMEM (Gibco [41965062]) complemented with 10% FBS (Sigma Aldrich [S0615]), L-glutamine (Sigma Aldrich [G7513]) and penicillin/streptomycin (Invitrogen [15140122]). MCF10A p53−/− cells were cultured in DMEM/F12 (Gibco [11330057]) supplemented with 10% heat-inactivated horse serum (Gibco [26050088]), penicillin/streptomycin, 100 ng/mL cholera toxin (Sigma Aldrich [C8052]), 20 ng/mL recombinant human EGF (animal-free; PeproTech [AF-100-15]), 0.5 mg/mL hydrocortisone (Sigma Aldrich [H0888]), and 10 μg/mL human recombinant insulin (Sigma Aldrich [91077C]). Cells were tested for mycoplasma contamination regularly using the Venor GeM Classic kit (Minerva Biolabs).

Microbe stains
DH5a and stbl3 bacteria were cultured in LB with corresponding antibiotics after transfected with recombinant plasmid in 37°C incubator.

METHOD DETAILS

Construct design
BTB$_{BCL6}$ and EGFR amino acid sequences were downloaded from UniProt (BCL6 [amino acids 5–129]: A5PL18; EGFR: P00533). For the BTB$_{BCL6}$-GFP fusion construct, the BTB$_{BCL6}$ domain sequence was introduced in the pArtichoke vector for expression in mammalian cells via Gateway cloning. BTB$_{BCL6}$ and GFP were connected by two flexible linkers (GGGS). For the EGFR-BTB$_{BCL6}$

fusion, BTB_{BCL6} was introduced at amino acid position 81 of the EGFR sequence with a flexible linker (GGGS)*2 attached. Additionally, the extracellular domain was replaced by a CD8 signaling peptide and a Myc tag. Fusion constructs were synthesized and cloned into the pArtichoke vector for expression in mammalian cells by Twist Bioscience. pArtichoke was a gift from Benjamin Ebert (Addgene plasmid #73320; http://n2t.net/addgene:73320; RRID: Addgene_73320).

Negative stain

Strep·Tag II-Avi–BCL6 (amino acids 5-360) was produced as previously described (Slabicki et al., 2020). To prepare grids for negative stain electron microscopy analysis of BCL6, strep·Tag II-Avi–BCL6 (amino acids 5-360) (1.75 mg/mL, 40 μM) in buffer (25 mM HEPES pH 7.4, 200 mM NaCl, 1 mM TCEP) was incubated with DMSO, 2 μM BI-3802, or 60 μM BI-3802 for 1 hour at room temperature and processed as previously described (Slabicki et al., 2020).

Estimation of BTB_{BCL6} polymer size

Negative stain micrographs of BTB_{BCL6} polymers with different concentrations of BI-3802 were imported into RELION 3.1 (Scheres, 2012; Zivanov et al., 2020). Using helical manual picking, the start and endpoints of the polymer fibers were recorded for all complete fibers within the micrograph boundaries. Completely bent fibers were rejected. The scale bar on the micrographs was used to scale pixel distances to nm. To estimate the number of BTB_{BCL6} dimers, polymer models with up to 73 dimers were constructed by sequentially extending the cryo-electron microscopy structure of BCL6 bound to BI-3802 (PDB 6XMX) in PyMOL 2.5.1 (The PyMOL Molecular Graphics System, 2010, Version 2.5.1 Schrödinger, LLC.). The polymer models were resized and superimposed onto longer fibers in the micrographs, and the start and endpoints were marked on 10 fibers to get an average distance of 2.13 nm per dimer. The maximum difference in fiber length estimate for 73 dimers was 6.3 nm, which translated to an error of approximately three per 73 dimers caused by fiber bending, micrograph resolution, and manual clicking error. Finally, from fiber length, kernel density estimation was used to gauge the number of dimers per fiber.

TR-FRET

Biotinylated BCL6 (amino acids 5-360) and Bodipy FL-labeled BCL6 (amino acids 5-360) were produced as described previously (Slabicki et al., 2020). Titrations of BI-3802 to induce BCL6 (amino acids 5-360) oligomerization were carried out by mixing 200 nM biotinylated BCL6 (amino acids 5-360), 200 nM Bodipy FL-labeled BCL6 (amino acids 5-360), and 2 nM terbium-coupled streptavidin (Invitrogen) in an assay buffer containing 50 mM Tris pH 8.0, 200 mM NaCl, 0.1% Pluronic F-68 solution (Sigma), 0.5% bovine serum albumin (w/v) and 1 mM TCEP. After dispensing the assay mixture (15 μL volume), increasing concentrations of compounds were dispensed in a 384-well microplate (Corning, 4514) using a D300e Digital Dispenser (HP), normalized to 1% DMSO. After excitation of terbium fluorescence at 337 nm, emission at 490 nm (terbium) and 520 nm (Bodipy FL) were recorded with a 70-μs delay over 600 μs to reduce background fluorescence, and the reaction was followed over 60 cycles of each data point using a PHERAstar FS microplate reader (BMG Labtech). The TR-FRET signal of each data point was extracted by calculating the 520/490 nm ratio. EC50 values were estimated using dose-response PRISM analysis.

Lentivirus production

1 × 10^6 HEK293T cells were seeded in a 10-cm dish in 10 mL medium. The next day, 3 μL TransIT-LT1 (Mirus [MIR2305]) were added to 15 μL OPTI-MEM (Invitrogen), incubated for 10 minutes, and combined with a mix consisting of 1000 ng of the desired expression plasmid, 500 ng psPAX2, and 50 ng pVSV-G in 32.5 μL OPTI-MEM. The solution was incubated for 30 minutes at room temperature, and 50 μL were added to HEK293T cells in a dropwise manner. After 16 hours, the medium was removed and replaced with 3 mL medium. On days 3 and 4, lentivirus-containing medium was collected and pooled. The virus was then further concentrated using the Lenti-XTM Concentrator (Takara Bio) according to manufacturer's instruction. The concentrated virus was resuspended in medium and stored at −80°C.

Lentiviral transduction

Cells were infected by spin infection. 0.5 × 10^6 cells were seeded in a 6-well plate one day before transduction. 20% (volume/volume) of the virus was added together with 0.8 μg/mL polybrene (Sigma [TR-1003]). Plates were centrifuged for two hours with 2,400 revolutions per minute (rpm) at 37°C. The virus was washed off 24 hours after infection.

Fluorescence-activated cell sorting

Lentivirally transduced HEK293T and MCF10A p53−/− cells were trypsinized, filtered through a 40-μm cell strainer (Corning), centrifuged with 1,200 rpm for four minutes, and resuspended in PBS supplemented with 2% FBS or horse serum. Live single cells co-expressing GFP and mCherry were sorted using a FACSAria I (BD Biosciences) and transferred back to cell culture medium.

Immunoblotting

HEK293T and MCF10A cells were treated as indicated in the figure legends. For lysate preparation, medium was removed, cells were washed with cold PBS (Gibco) and scraped on ice. Cells were transferred to 2-mL microcentrifuge tubes and pelleted at 13,000 rpm for 10 seconds in a precooled microcentrifuge. Supernatant was removed, and samples were immediately transferred to dry ice. After

thawing on ice, cell pellets were resuspended in RIPA buffer (Pierce) supplemented with HALT Protease and HALT Phosphatase Inhibitor (1:100; ThermoFisher) and benzonase (1:1000; Merck Millipore [71205-3]) and incubated on ice for 30 minutes. The soluble fraction (protein lysate) was separated by centrifugation with 13,000 rpm at 4°C for 10 minutes, transferred to Qiashredder columns (Qiagen), and centrifuged with 13,000 rpm at 4°C for 2 minutes. The protein concentration of the cleared lysates was assessed using Protein Assay Dye Reagent Concentrate (Bio-Rad). For immunoblotting, lysates containing 40-50 μg protein were mixed with NuPAGE LDS Sample Buffer and NuPAGE Sample Reducing Agent (Life Technologies), denatured at 95°C for 5 minutes, and resolved on 10% SDS-polyacrylamide gels (Bio-Rad) by electrophoresis. Proteins were transferred to membranes using the Trans-Blot Turbo Transfer System (Bio-Rad), and the membranes were incubated with the indicated antibodies and visualized using an Odyssey CLx device (LiCor).

Colony formation
Cells were trypsinized, filtered through a 40-μm cell strainer (Corning), and counted. 1,500 cells were seeded in 2 mL culture medium in tissue culture-treated 6-well plates and incubated at 37°C for seven days. Each sample was seeded in duplicate. Medium was changed every two to three days. At readout, medium was removed, plates were transferred to ice, washed with cold PBS, and fixed with ice-cold methanol for 15 minutes. Methanol was removed, and cells were incubated with 2.5 % crystal violet solution (Sigma [C6158]) at room temperature for 20 minutes. Wells were washed repeatedly with deionized water to remove excess staining solution. After drying, plates were scanned, and the cell-covered area of each well was quantified using ImageJ.

Live cell imaging
1×10^3 cells/mL were seeded in a μ-Slide 8 Well Chamber (ibidi) and cultured under standard growth conditions for 18 to 24 hours. Cell culture medium was replaced with CO_2-independent medium (Gibco), and cells were imaged with a Leica DMi8 microscope. The Blue OPSL 488-nm laser using PMT SP confocal detectors for imaging and transmitted light PMT for bright-field images were used. To capture foci within a cell, around 26 μm per cell were imaged every 0.4 and 0.5 μm. Images were pre-analyzed using Leica Application Suite X Software and further analyzed using ImageJ.

QUANTIFICATION AND STATISTICAL ANALYSIS

TR-FRET analysis
The TR-FRET signal of each data point was extracted by calculating the 520/490 nm ratio. EC50 values were estimated using dose-response GraphPad PRISM analysis. Dots represent the mean; error bars SD. Lines represent the standard four-parameter log-logistic curve. Statistical details can be found in the figure legend of Figure 1D.

Foci quantification
The number of foci was quantified by manual picking using ImageJ (Figure S2C). Data was analyzed using GraphPad PRISM. Bars represent the mean; error bars depict SD. N represents the number of independent experiments. Further statistical details are depicted in the figure legend.

Western Blot quantification
Quantification of western blot band intensities (Figures 3B and 3D) was performed using Image Studio Lite software (version 5.2.5; LI-COR). Lines represent the median. N represents the number of independent experiments. Further details are described in the figure legends.

Colony formation assay
Statistical analysis for the colony formation results shown in Figure 3C was performed by one-way ANOVA with Dunnett's multiple comparison test (test conditions compared to control) using GraphPad Prism (version 8.4.2; GraphPad Software). Lines represent the median. N represents the number of independent experiments. Further details are described in the figure legend.